

Anomalous normal stress controlled by marginal stability in fiber networks

Jordan Shivers,^{1,2} Jingchen Feng,² Abhinav Sharma,³ and Fred C. MacKintosh^{1,2,4}

¹*Department of Chemical and Biomolecular Engineering, Rice University, Houston, TX 77005, USA*

²*Center for Theoretical Biological Physics, Rice University, Houston, TX 77030, USA*

³*Leibniz-Institut für Polymerforschung Dresden, 01069 Dresden, Germany*

⁴*Departments of Chemistry and Physics & Astronomy, Rice University, Houston, TX 77005, USA*

As first identified by Poynting, typical elastic solids exhibit axial extension under torsion. Along with related normal stress effects such as rod climbing of non-Newtonian fluids, this depends on the first normal stress difference N_1 , which is of fundamental importance for a variety of nonlinear deformation and flow phenomena, especially in soft matter. This stress difference is almost always positive for elastic solids and viscoelastic polymer materials. Recent work has shown that biopolymer networks can exhibit negative normal stress, but whether N_1 itself can be negative in these networks remains an open question. We demonstrate that lattice-based 2D and 3D fiber network models, as well as off-lattice 2D networks, can indeed exhibit an anomalous negative N_1 . We also show that this anomaly becomes most pronounced near a critical point of marginal stability, suggesting the importance of critical fluctuations in driving the change of sign in N_1 . Finally, we present a phase diagram indicating regimes of anomalous normal stress as a function of strain, network connectivity, and disorder.

Normal solids and liquids exhibit shear stress when subject to deformation. With the exception of simple Newtonian liquids, most real materials also develop so-called normal stresses in response to shear. Unlike shear stress, however, these stresses are directed perpendicular to surface on which they act, and they appear as diagonal terms in the stress tensor. In the case of elastic solids, a common manifestation of normal stress is the Poynting effect, in which a solid tends to elongate in response to torsional strain [1]. In a classic series of experiments, Poynting observed such elongation for a variety of systems, ranging from simple metal wires to rubber [1, 2]. By symmetry, this elongation should not depend on the sign or direction of the applied torsion, leading to lowest-order response that is expected to be quadratic in the strain, making the Poynting effect a fundamentally nonlinear phenomenon. This is also a reason why normal stresses are typically less apparent than, e.g., the shear stress that varies linearly with strain. Nevertheless, normal stresses have very dramatic consequences, including both rod climbing and tubeless siphoning, as well as die swell [3].

Microscopically, these phenomena depend on differences between the various diagonal terms in the stress tensor, and especially the first normal stress difference $N_1 = \sigma_{xx} - \sigma_{zz}$, where x represents the direction of flow/deformation and z is the flow/deformation gradient direction. This quantity is fundamental to the nonlinear (visco)elastic response of materials and is almost universally positive, particularly for solids. Here, we demonstrate that fiber networks are predicted to exhibit an anomalous negative N_1 and that this anomaly is most pronounced near the point of marginal stability as a function of strain, which corresponds to a critical point. Using disordered 2D and 3D lattice-based models as well as the off-lattice 2D Mikado model, we show that the sign of N_1 depends on the network connectivity and level of applied strain. These observations point to the important role of critical fluctuations as the origin of the anomalous normal stress. Our results suggest that biopolymer gels, and especially collagen matrices,

may exhibit negative normal stress even in the incompressible limit.

Both the Poynting effect in solids as well as die swell and rod climbing in non-Newtonian liquids correspond to positive normal stress. Fundamentally, the measured normal stress in torsion depends not only on the axial stress component σ_{zz} , but also on the azimuthal component σ_{xx} , due to the hoop stress it generates. Thus, for a torsional cone-plate rheometer, the sign of N_1 determines the sign of the measured axial force for incompressible systems. For polymer networks, N_1 is expected to be positive [4], because polymer extension in the azimuthal direction tends to be greater than in the axial direction. It was thus surprising when biopolymer gels were recently identified as apparent exceptions to this, with an inverted or negative Poynting effect [5]. However, as recently demonstrated by de Cagny et al., this anomaly for fibrin gels can be understood to arise from the porous, two-component nature of such hydrogels, which renders the networks effectively compressible on long enough time scales. Consistent with this interpretation, these networks showed a normal (positive) Poynting effect on short enough time scales, where the gels become effectively incompressible, indicating that the normal stress difference N_1 remains positive for fibrin gels. Thus, we ask whether it is possible to have $N_1 < 0$ in an elastic solid. This has not yet been demonstrated.

To address this, we study a variety of computational network models in both 2D and 3D. We construct disordered lattice-based networks in 2D beginning with a triangular lattice with spacing $l_0 = 1$ [6, 7], which we then *phantomize* in order to reduce the average network connectivity $\langle z \rangle$ to 4 [8]. This is done by disconnecting one of three intersecting fibers at each node. We further dilute the network, randomly removing bonds to achieve the desired network connectivity after the removal of dangling ends. These steps ensure that the local connectivity does not exceed a physical maximum of 4 (two crosslinked fibers). Models constructed in this way have been shown to accurately describe the shear elasticity of

physiological collagen networks [9], which have a typical average value of $\langle z \rangle \approx 3.4$ [10]. Our bond dilution procedure introduces disorder in the network's local connectivity, but still leaves long, perfectly straight fibers in the unstrained state.

With an eye toward modeling collagen networks, which are disordered not only in local connectivity but also in fiber bending (Fig. 1a), we introduce geometric distortion to the unstrained lattice network by moving each node a random distance in the range $[0, \delta_{\max}]$ in a random direction, with $\delta_{\max} \leq 0.5$ in order to avoid overlapping nodes [11–13]. Subsequently, the rest lengths $l_{ij,0}$ between pairs of nodes and rest angles $\theta_{ijk,0}$ between connected triplets of nodes are reset so that the geometrically disordered network exhibits zero stress in the unstrained state. The process for generating disordered 3D networks is similar, but begins with a face-centered cubic (FCC) lattice [14, 15]. In this way, we construct disordered 2D and 3D networks with the same average connectivity. Examples of these are shown in Fig. 1b and c. In addition to these lattice-based networks, we also construct Mikado networks by placing straight segments of length L with random positions and orientations into a 2D periodic box, adding crosslinks at the intersections between segments, and removing dangling ends [16, 17].

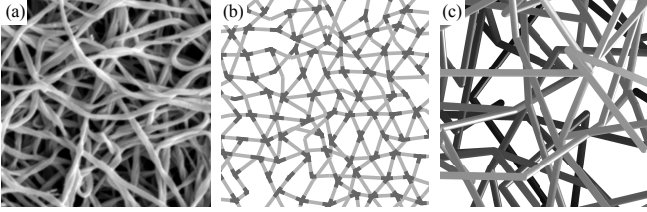


FIG. 1. (A) Image of an unstrained sample of a collagen network, exhibiting clear connective and geometric disorder, adapted from Ref. [9]. (b) Portions of a bond-diluted phantom 2D network and (c) 3D FCC network, both unstrained and with added geometric disorder $\delta_{\max} = 0.4$.

Each fiber in the network is modeled as a discretized extensible worm-like chain (EWLC) [17]. This model treats individual bonds as Hookean springs with stretching modulus μ and pairs of consecutive bonds with bending modulus κ . The Hamiltonian \mathcal{H} of the full network, summed over all fibers f , is

$$\mathcal{H} = \frac{1}{W^d} \sum_f \left[\frac{\mu}{2} \sum_{\langle ij \rangle} \frac{(l_{ij} - l_{ij,0})^2}{l_{ij,0}} + \frac{\kappa}{2} \sum_{\langle ijk \rangle} \frac{(\theta_{ijk} - \theta_{ijk,0})^2}{l_{ijk,0}} \right], \quad (1)$$

in which the inner sums are taken over pairs $\langle ij \rangle$ and triplets $\langle ijk \rangle$ of connected nodes along each fiber, and $l_{ijk,0} = (l_{ij} + l_{jk})/2$. Here, W is the side-length of the network and d is the dimensionality of the system. Results reported here correspond to $W = 120$ for 2D lattice networks and $W = 30$ for 3D. As in prior work, we define a dimensionless bending rigidity $\tilde{\kappa} = \kappa/\mu l^2$, with characteristic length l . For 2D and 3D lattice networks, this length is the lattice spacing, $l = l_0 = 1$.

For Mikado networks, $l = l_c$, where l_c is the average distance between crosslinks [18].

We perform simulations of networks under simple shear by incrementally increasing the shear strain γ from 10^{-3} to 10 in logarithmically spaced steps, using Lees-Edwards periodic boundary conditions [19]. For simplicity of notation when comparing 2D and 3D simulations, we call x and z the directions of shear and gradient, respectively, in both cases. At each strain value, the network energy is minimized using the conjugate gradient method [20], and each component of the stress tensor σ is computed as

$$\sigma_{\alpha\beta} = \frac{1}{2W^d} \sum_{\langle ij \rangle} f_{ij,\alpha} u_{ij,\beta} \quad (2)$$

in which $\mathbf{u}_{ij} = \mathbf{u}_j - \mathbf{u}_i$ is the vector between nodes i and j and \mathbf{f}_{ij} is the force acting on node i due to node j [21].

For comparison, we also consider the limit of an isotropic medium composed of linear springs of length $l_0 = 1$ oriented initially in all directions, which are assumed to deform affinely under simple shear. This yields an analytical prediction for the behavior of the full stress tensor of a disordered network in the affine, stretch-dominated regime in both 2D and 3D. This model exhibits the expected behavior for a typical elastic material: both normal stress components increase as γ^2 , as required by symmetry, and $\sigma_{xx} > \sigma_{zz}$, resulting in $N_1 > 0$ for all values of γ . Furthermore, this model satisfies the Lodge-Meissner relation [4], in which $N_1 = \sigma_{xz}\gamma$ for an affinely deforming Gaussian network. Predictions from the affine model are shown as solid lines in Fig. 2 and 3.

For disordered networks with $\langle z \rangle = 3.6$, $\delta_{\max} = 0.4$, and varying values of $\tilde{\kappa}$, we find that the normal stress components σ_{xx} and σ_{zz} increase monotonically with strain, initially with both σ_{xx} and σ_{zz} proportional to $\tilde{\kappa}\gamma^2$, as shown in Fig. 2a. This is consistent with a bend-dominated regime at low strain [12, 17, 22, 23], which is shown more directly in Fig. 2b. At higher strain, the response becomes stretch dominated and the various stress components converge to the affine values, with $\sigma_{xx} \propto \mu\gamma^2$ and $\sigma_{zz} \propto \mu$ (Fig. 2a). The transition from the bend-dominated regime to the stretch-dominated regime occurs at the critical strain γ_c , and this transition becomes sharper with decreasing $\tilde{\kappa}$. We determine the value of the critical strain as in prior work [9], defining it independently of the normal stresses as the logarithmic inflection point of the K vs. γ curve, in which $K = \partial\sigma_{xz}/\partial\gamma$ (Fig. 2b, inset).

Surprisingly, we find that for certain values of network connectivity, $\sigma_{xx} < \sigma_{zz}$ over a wide range of strain values, corresponding to a negative N_1 (Fig. 2c and d). Here, N_1 is negative with magnitude proportional to $\tilde{\kappa}$ in the bend-dominated regime, increases in magnitude in the vicinity of the critical strain γ_c , and is independent of $\tilde{\kappa}$ in the stretch-dominated regime. At $\gamma \approx 25\%$, N_1 becomes positive irrespective of the network connectivity. The ratio of the normal stresses, σ_{zz}/σ_{xx} , which is largely independent of $\tilde{\kappa}$ aside from a $\tilde{\kappa}$ -dependent peak at the critical strain, depicts this transition cleanly (Fig. 2c and d, inset); when σ_{zz}/σ_{xx} becomes less than

1, N_1 becomes positive. Since this ratio is independent of $\bar{\kappa}$ except near the critical strain, the same is true of N_1 : outside of a narrow strain window around the critical strain, N_1 depends only on the network geometry, i.e., the connectivity and imposed distortion. 2D and 3D networks with the same connectivity and imposed distortion show the same negative N_1 behavior (Fig. 2c and d).

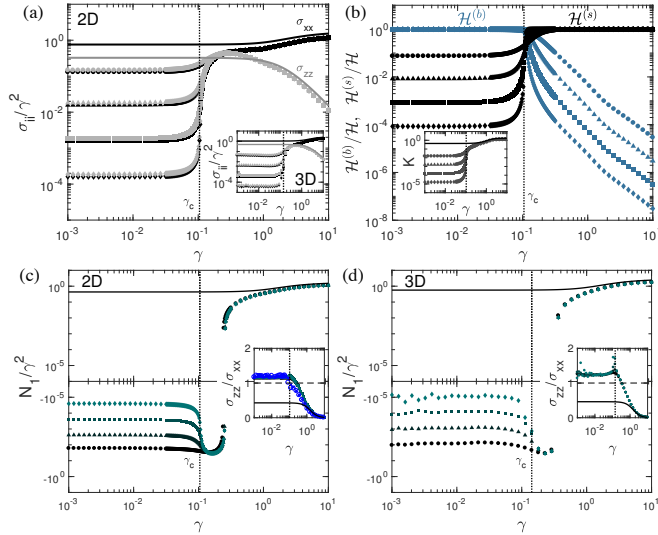


FIG. 2. 2D and 3D distorted ($\delta_{\max} = 0.4$) lattice networks and Mikado networks exhibit negative N_1 . (a) Normal stress components σ_{xx} (black) and σ_{zz} (gray) normalized by γ^2 for 2D and (inset) 3D networks with average connectivity $\langle z \rangle = 3.6$ and reduced bending rigidity $\bar{\kappa} = 10^{-3}$ (\bullet), 10^{-4} (\blacktriangle), 10^{-5} (\blacksquare), and 10^{-6} (\blacklozenge). The same quantities determined for the affine model are shown as thick solid lines, and the critical strain γ_c is shown as a dotted line in all panels. (b) The ratios of the stretching ($\mathcal{H}^{(s)}$) and bending ($\mathcal{H}^{(b)}$) energies to the total network energy \mathcal{H} as a function of strain, for the same 2D networks as in (a), clearly transition from being bending-dominated to stretching-dominated at γ_c . Inset: The corresponding differential shear modulus K is shown as a function of γ . Most of the strain stiffening apparent in K appears before the transition to stretch-dominated behavior at γ_c (dotted line). (c) Merged positive and negative (inverted axis) log-log plots of N_1 normalized by γ^2 for 2D distorted lattice networks with varying $\bar{\kappa}$. The measured N_1 approaches that of the affine model (solid line) at high strain. Inset: The ratio of the normal stress components σ_{zz}/σ_{xx} is independent of $\bar{\kappa}$ apart from a peak at the critical strain. Blue results correspond to Mikado networks with $\langle z \rangle = 3.6$ and $\bar{\kappa} = 10^{-4}$ (\times) and 10^{-5} (\circ), which yield approximately the same σ_{zz}/σ_{xx} ratio and hence negative N_1 at low strain. (d) 3D distorted lattice networks with $\langle z \rangle = 3.6$ show the same behavior in N_1 and yield a similar ratio of the normal stress components at low strain.

We further compare the measured values of N_1 shown in Fig. 2 to the affine limit by plotting N_1 normalized by the Lodge-Meissner relation, which predicts $N_1 = \sigma_{xz}\gamma$. We find that for a particular network connectivity and disorder, $N_1/(\sigma_{xz}\gamma)$ is constant in the low-strain bend-dominated regime and equal to 1 in the high-strain stretch-dominated regime, in which the network behaves according to the affine model. At low strain, this ratio becomes increasingly negative

with increasing $\langle z \rangle$. This can be understood in terms of the nonaffinity, as higher nonaffinity should correspond to greater deviation from the (affine) Lodge-Meissner relation, and prior work has shown that nonaffine fluctuations in the linear regime become stronger as the network connectivity approaches the central force isostatic point (corresponding to $\langle z \rangle = 4$ in 2D) [24]. Further supporting the idea that nonaffine fluctuations determine the sign of N_1 , this ratio has a negative peak at the critical strain γ_c . This is expected, as networks exhibit maximal nonaffine strain fluctuations at the critical strain [9, 18], and thus we expect the normal stress difference at the critical strain to most strongly violate the Lodge-Meissner relation. This peak shifts with γ_c for different values of $\langle z \rangle$ (Fig. 3b).

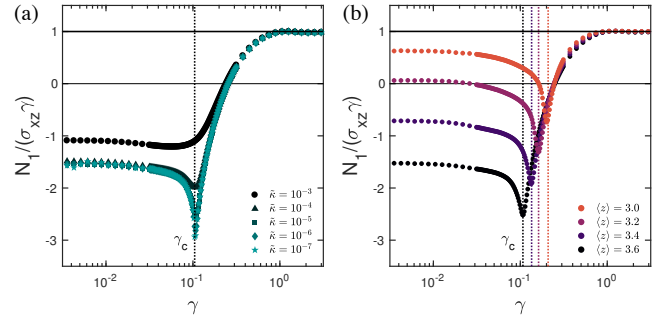


FIG. 3. First normal stress difference normalized by the Lodge-Meissner relation ($N_1 = \sigma_{xz}\gamma$) in 2D distorted lattice networks ($\delta_{\max} = 0.4$) as a function of γ for (a) $\langle z \rangle = 3.6$ and varied $\bar{\kappa}$ and (b) $\bar{\kappa} = 10^{-5}$ and varied $\langle z \rangle$, with the affine limit result ($N_1/(\sigma_{xz}\gamma) = 1$) shown as a thick solid line. For networks, the ratio is approximately constant in γ at low strain, with deviation from the Lodge-Meissner relation increasing with $\langle z \rangle$. This ratio exhibits a downward peak and maximal anomaly at the critical strain γ_c , which grows with decreasing $\bar{\kappa}$ and shifts with γ_c for varying $\langle z \rangle$. At high strain, ratios for all networks (irrespective of $\langle z \rangle$ and $\bar{\kappa}$) converge to the affine result.

In both the bend-dominated and stretch-dominated regimes, the sign of N_1 is independent of $\bar{\kappa}$. However, even for networks which exhibit positive N_1 in these regimes, large non-affine strain fluctuations near the critical strain γ_c can drive N_1 to become negative. This effect, apparent in Fig. 3b, becomes significant for networks with low values of $\bar{\kappa}$, which show increased nonaffine strain fluctuations at the critical strain relative to high- $\bar{\kappa}$ networks [9].

Having shown that the sign of N_1 depends on strain, connectivity, and imposed distortion, we construct phase diagrams depicting the sign of the N_1 as a function of $\langle z \rangle$ and δ_{\max} in the (small-strain) linear regime (Fig. 4a), and also as a function of $\langle z \rangle$ and γ for various values of δ_{\max} (Fig. 4b). For undistorted networks ($\delta_{\max} = 0$), we find that N_1 is initially positive in the small strain limit for all values of $\langle z \rangle$ (Fig. 4a). This seems to be an artifact of the ordered lattice structure, as slightly increasing δ_{\max} causes a range of high $\langle z \rangle$ values to exhibit negative N_1 . With sufficient disorder ($\delta_{\max} > 0.3$), the sign of N_1 at low strain becomes independent of δ_{\max} , depending only on connectivity. That the effect of δ_{\max} on the phase boundary becomes negligible at high δ_{\max} suggests that

our results are insensitive to the precise form of applied geometric disorder. The region of the phase diagram in Fig. 4a that we expect to be relevant to real collagen networks is the region with $\delta_{\max} > 0.3$, as these exhibit significant geometric disorder due to fiber bending.

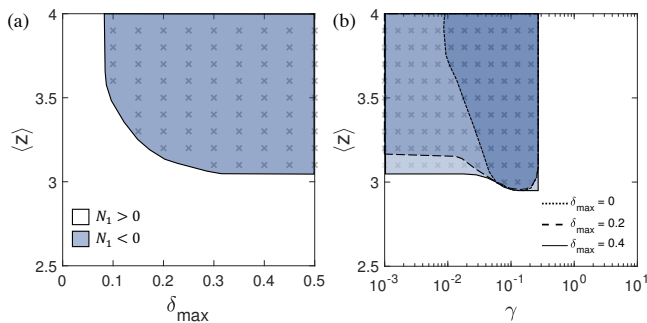


FIG. 4. (a) Phase diagram depicting the sign of N_1 in the low-strain limit ($\gamma = 10^{-3}$) as a function of connectivity $\langle z \rangle$ and imposed geometric distortion δ_{\max} , for 2D networks with $\bar{\kappa} = 10^{-3}$. While undistorted networks show positive N_1 in the low-strain limit for all values of $\langle z \rangle$, increasing δ_{\max} results in range of connectivities at which $N_1 < 0$, which grows quickly with distortion initially but becomes independent of distortion above $\delta_{\max} \approx 0.3$. (b) Sign of N_1 for the same networks as a function of connectivity and strain, with boundaries shown for different values of δ_{\max} . For sufficiently high distortion, the phase boundary is independent of strain in the linear regime. All networks exhibit positive N_1 above strains of $\gamma \approx 25\%$.

We also find that even undistorted lattices, for which N_1 is positive in the low strain limit, can exhibit negative N_1 at intermediate levels of applied strain (Fig. 4b) and values of $\langle z \rangle$ greater than 3. With sufficiently high geometric distortion, the phase boundary becomes independent of strain in the linear, bending-dominated regime. Importantly, this means that in the linear regime for networks with sufficient geometric disorder, the sign of N_1 depends only on $\langle z \rangle$, and is independent of the δ_{\max} , $\bar{\kappa}$, and γ . For all values of imposed distortion and connectivity, N_1 becomes positive for strains above $\gamma \approx 25\%$. Above this strain, N_1 converges to the high-strain affine isotropic model prediction for all values of $\langle z \rangle$ (Fig. 4b), independently of the critical strain (see Fig. 3b). This crossover strain is independent of $\langle z \rangle$, $\bar{\kappa}$, and δ_{\max} .

Here we have studied the behavior of normal stresses in 2D and 3D distorted network models and the 2D Mikado model as a function of strain, and have demonstrated that these networks can exhibit a negative first normal stress difference. Our results show that the sign of N_1 as a function of the strain can be tuned as a function of the network connectivity and geometric distortion, with an additional dependence on the fiber bending rigidity $\bar{\kappa}$ that appears only near the critical strain. Significantly, we find that with increasing geometric disorder the sign of the normal stress in the linear regime becomes independent of the properties of individual fibers ($\bar{\kappa}$) and the level of applied strain, depending only on the network connectivity. Further, we show that the sign of the normal stress can be controlled by nonaffine critical fluctuations; N_1 be-

comes increasingly negative both in the linear regime as one approaches the isostatic point ($\langle z \rangle = 4$) and, more generally, as γ approaches γ_c for subisostatic networks. As a result, even networks with positive N_1 in the bending and stretching-dominated regimes can be driven by nonaffine fluctuations to exhibit negative N_1 near the critical strain.

Our results suggest a surprising negative N_1 , and not just an inverted Poynting effect, in a model elastic solid. While negative N_1 under shear has been observed in liquid crystalline polymers [25] and shear thickening suspensions [26–28], observation of this effect in an elastic solid was unexpected. Moreover, this work suggests a new way to control the sign of the normal stress in elastic networks in the incompressible limit by approaching a point of marginal stability, i.e. a mechanical critical point, and thereby controlling the nonaffinity. Controlling the sign of N_1 could have significant applications; for example, die swell that is associated with positive N_1 often poses a significant impediment to the processing of various polymeric liquids. Although negative N_1 has not yet been observed experimentally in fiber networks, our results suggest that collagen networks, which are athermal, highly-disordered fiber networks with typical connectivity of $\langle z \rangle \approx 3.4$ [9, 10], could be candidates for this behavior.

This work was supported in part by the National Science Foundation Center for Theoretical Biological Physics (Grant PHY-1427654).

APPENDIX A: AFFINELY DEFORMING ISOTROPIC NETWORK MODEL

Consider a filament segment with initial orientation $\hat{\mathbf{n}}$, undergoing deformation described by the tensor $\Lambda(\gamma)$. The deformation changes the filament's length and orientation, resulting in a tension τ directed along its new orientation. Treating the filament as a linear elastic element with stretching modulus μ and initial length $l_0 = 1$, the tension vector is $\boldsymbol{\tau} = \tau \Lambda \hat{\mathbf{n}} / |\Lambda \hat{\mathbf{n}}|$, with $\tau = \mu(|\Lambda \hat{\mathbf{n}}| - 1)$. Taking the average, over all initial filament orientations, of the product of the i component of the tension, $\tau \Lambda_{il} n_l / |\Lambda \hat{\mathbf{n}}|$, and the line density of filaments crossing the j plane after the deformation, $\frac{\rho}{\det \Lambda} \Lambda_{jk} n_k$, yields the stress tensor [29, 30],

$$\sigma_{ij} = \frac{\rho}{\det \Lambda} \left\langle \tau \frac{\Lambda_{il} n_l \Lambda_{jk} n_k}{|\Lambda \hat{\mathbf{n}}|} \right\rangle, \quad (3)$$

Since we consider only volume-conserving simple shear, $\det \Lambda = 1$. Thus, for filaments in 3D with initial polar angle θ and azimuthal angle φ , the stress tensor is

$$\sigma_{ij} = \frac{\rho}{4\pi} \int_{\varphi} \int_{\theta} d\theta d\varphi \sin \theta \left[\tau \frac{\Lambda_{il} n_l \Lambda_{jk} n_k}{|\Lambda \hat{\mathbf{n}}|} \right], \quad (4)$$

in which the deformation tensor for simple shear in 3D is

$$\Lambda(\gamma) = \begin{pmatrix} 1 & 0 & \gamma \\ 0 & 1 & 0 \\ 0 & 0 & 1 \end{pmatrix} \quad (5)$$

and the transformed orientation vector is

$$\mathbf{\Lambda}\hat{\mathbf{n}} = \begin{pmatrix} \sin\theta \cos\varphi + \gamma \cos\theta \\ \sin\theta \sin\varphi \\ \cos\theta \end{pmatrix}. \quad (6)$$

We compute the xz , xx , and zz components of the stress tensor for the 3D case as follows:

$$\sigma_{xz} = \frac{\rho}{4\pi} \int_{\varphi} \int_{\theta} d\theta d\varphi \sin\theta \left[\tau \frac{(\sin\theta \cos\varphi + \gamma \cos\theta) \cos\theta}{|\mathbf{\Lambda}\hat{\mathbf{n}}|} \right] \quad (7)$$

$$\sigma_{xx} = \frac{\rho}{4\pi} \int_{\varphi} \int_{\theta} d\theta d\varphi \sin\theta \left[\tau \frac{(\sin\theta \cos\varphi + \gamma \cos\theta)^2}{|\mathbf{\Lambda}\hat{\mathbf{n}}|} \right] \quad (8)$$

$$\sigma_{zz} = \frac{\rho}{4\pi} \int_{\varphi} \int_{\theta} d\theta d\varphi \sin\theta \left[\tau \frac{\cos^2\theta}{|\mathbf{\Lambda}\hat{\mathbf{n}}|} \right] \quad (9)$$

The integrals are taken over the ranges $0 \leq \theta \leq 2\pi$ and $0 \leq \varphi \leq \pi$. To compare with our results for the 3D FCC network, we use $\mu = 1$ and initial line density $\rho = \frac{12}{\sqrt{2}}$, corresponding to the fully-connected FCC lattice with $l_0 = 1$ [31].

We repeat the same process for the 2D case, in which the deformation tensor for simple shear is

$$\mathbf{\Lambda}(\gamma) = \begin{pmatrix} 1 & \gamma \\ 0 & 1 \end{pmatrix} \quad (10)$$

and the transformed orientation vector is

$$\mathbf{\Lambda}\hat{\mathbf{n}} = \begin{pmatrix} \cos\theta + \gamma \sin\theta \\ \sin\theta \end{pmatrix}. \quad (11)$$

The resulting components of the 2D stress tensor are calculated as follows:

$$\sigma_{xz} = \frac{\rho}{2\pi} \int_{\theta} d\theta \left[\tau \frac{(\cos\theta + \gamma \sin\theta) \sin\theta}{|\mathbf{\Lambda}\hat{\mathbf{n}}|} \right] \quad (12)$$

$$\sigma_{xx} = \frac{\rho}{2\pi} \int_{\theta} d\theta \left[\tau \frac{(\cos\theta + \gamma \sin\theta)^2}{|\mathbf{\Lambda}\hat{\mathbf{n}}|} \right] \quad (13)$$

$$\sigma_{zz} = \frac{\rho}{2\pi} \int_{\theta} d\theta \left[\tau \frac{\sin^2\theta}{|\mathbf{\Lambda}\hat{\mathbf{n}}|} \right] \quad (14)$$

Here, the integrals are taken over the range $0 \leq \theta \leq 2\pi$. For comparison with our 2D lattice simulations, we use $\mu = 1$ and $\rho = \frac{6}{\sqrt{3}}$, corresponding to the fully-connected triangular lattice with $l_0 = 1$ [31].

APPENDIX B: STRAIN-SCALING OF THE NORMAL STRESS COMPONENTS

Figure 5 shows the scaling of the normal stress components at low and high strain for 2D distorted lattice networks and for

the 2D affine model, with a larger upper strain limit than in Figure 2. For distorted lattice networks in the low-strain limit, both normal stress components are proportional to the bending rigidity κ and quadratic in strain. For the affine model, which lacks bending, the normal stress components are both proportional to $\mu\gamma^2$ in the low-strain limit. In the high-strain limit, the normal stress components for both the distorted lattice networks and the affine model are proportional to the stretching modulus μ . In this limit, the xx component remains quadratic in the strain whereas the zz component is constant.

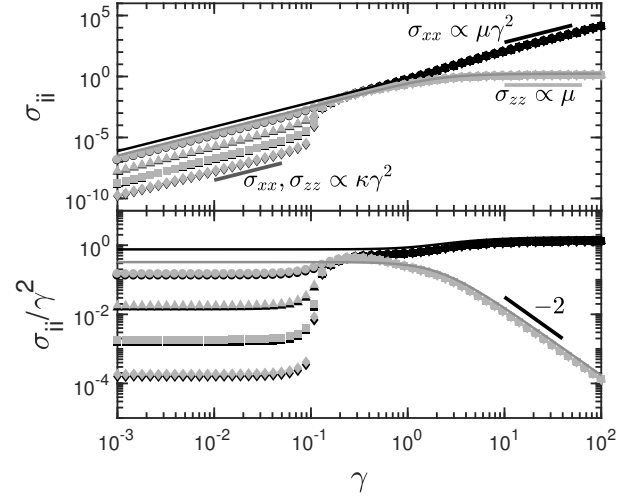


FIG. 5. Top: Normal stress components σ_{xx} (black) and σ_{zz} (gray) for 2D networks with average connectivity $\langle z \rangle = 3.6$, distortion $\delta_{\max} = 0.4$, and reduced bending rigidity $\tilde{\kappa} = 10^{-3}$ (\bullet), 10^{-4} (\blacktriangle), 10^{-5} (\blacksquare), and 10^{-6} (\blacklozenge). The normal components of the stress tensor for the affine isotropic network model are shown as solid lines. In the low strain limit, both normal stress components are proportional to $\kappa\gamma^2$ for the networks and $\mu\gamma^2$ for the affine model. At high strain, $\sigma_{xx} \propto \mu\gamma^2$ and $\sigma_{zz} \propto \mu$ for both the networks and the affine model. Bottom: The same data are shown normalized by γ^2 .

- [1] J. H. Poynting, Proceedings of the Royal Society of London. Series A **82**, 546 (1909).
- [2] J. H. Poynting, The India-Rubber Journal, 6 (1913).
- [3] R. G. Larson, *The Structure and Rheology of Complex Fluids* (Oxford University Press, New York, USA, 1999).
- [4] A. S. Lodge and J. Meissner, Rheologica Acta **11**, 351 (1972).
- [5] P. A. Janmey, M. E. McCormick, S. Rammensee, J. L. Leight, P. C. Georges, and F. C. MacKintosh, Nature Materials **6**, 48 (2007).
- [6] M. F. Thorpe, Journal of Non-Crystalline Solids **76**, 109 (1985).
- [7] M. Das, F. C. MacKintosh, and A. J. Levine, Physical Review Letters **99**, 038101 (2007).
- [8] C. P. Broedersz and F. C. MacKintosh, Soft Matter **7**, 3186 (2011).
- [9] A. Sharma, A. J. Licup, K. A. Jansen, R. Rens, M. Sheinman, G. H. Koenderink, and F. C. MacKintosh, Nature Physics **12**, 584 (2016).

- [10] S. B. Lindström, D. A. Vader, A. Kulachenko, and D. A. Weitz, *Physical Review E* **82**, 051905 (2010).
- [11] D. J. Jacobs and M. F. Thorpe, *Physical Review E* **53**, 3682 (1996).
- [12] P. R. Onck, T. Koeman, T. van Dillen, and E. van der Giessen, *Physical Review Letters* **95**, 178102 (2005).
- [13] R. Rens, M. Vahabi, A. J. Licup, F. C. MacKintosh, and A. Sharma, *Journal of Physical Chemistry B* **120**, 5831 (2016).
- [14] S. Feng and P. N. Sen, *Physical Review Letters* **52**, 216 (1984).
- [15] C. P. Broedersz, M. Sheinman, and F. C. MacKintosh, *Physical Review Letters* **108**, 078102 (2012).
- [16] J. Wilhelm and E. Frey, *Physical Review Letters* **91**, 108103 (2003).
- [17] D. A. Head, A. J. Levine, and F. C. MacKintosh, *Physical Review Letters* **91**, 108102 (2003).
- [18] A. Sharma, A. J. Licup, R. Rens, M. Vahabi, K. A. Jansen, G. H. Koenderink, and F. C. MacKintosh, *Physical Review E* **94**, 042407 (2016).
- [19] A. W. Lees and S. F. Edwards, *Journal of Physics C: Solid State Physics* **5**, 1921 (1972).
- [20] W. H. Press, B. P. Flannery, S. A. Teukolsky, and W. T. Vetterling, *Numerical Recipes in C: The Art of Scientific Computing*, 2nd ed. (Cambridge University Press, 1992) pp. 420–425.
- [21] M. Doi and S. F. Edwards, *The Theory of Polymer Dynamics*, Vol. 73 (Oxford University Press, 1988).
- [22] R. L. Satcher and C. F. Dewey, *Biophysical Journal* **71**, 109 (1996).
- [23] K. Kroy and E. Frey, *Physical Review Letters* **77**, 306 (1996).
- [24] C. P. Broedersz, X. Mao, T. C. Lubensky, and F. C. MacKintosh, *Nature Physics* **7**, 983 (2011).
- [25] G. Kiss and R. S. Porter, *Journal of Polymer Science: Polymer Physics Edition* **18**, 361 (1980).
- [26] D. R. Foss and J. F. Brady, *Journal of Fluid Mechanics* **407**, 167 (2000).
- [27] M. Lee, M. Alcoutlabi, J. J. Magda, C. Dibble, M. J. Solomon, X. Shi, and G. B. McKenna, *Journal of Rheology* **50**, 293 (2006).
- [28] C. D. Cwalina and N. J. Wagner, *Journal of Rheology* **58**, 949 (2014).
- [29] C. Storm, J. J. Pastore, F. C. MacKintosh, T. C. Lubensky, and P. A. Janmey, *Nature* **435**, 191 (2005).
- [30] C. P. Broedersz, C. Storm, and F. C. MacKintosh, *Physical Review E* **79**, 1 (2009).
- [31] A. J. Licup, A. Sharma, and F. C. MacKintosh, *Physical Review E* **93**, 1 (2016).